IEEE Robotics and Automation Letters (RAL) paper presented at
2024 IEEE/RSJ International Conference on Intelligent Robots and Systems (IROS)
October 14-18, 2024. Abu Dhabi, UAE

Novel Lightweight Lower Limb Exoskeleton Design for Single-Motor Sequential Assistance of Knee & Ankle Joints in Real World

Xinyu Wu[1] ,*Graduate Student Member,IEEE,* Aibin Zhu[1] , *Member,IEEE*, Xiao Li[2] , Bingsheng Bao[1] , Jing Zhang[1] , Lei Shi[2] , Diyang Dang[3] and Peng Xu[4]

***Abstract*—In this paper, we introduce a lightweight lower limb exoskeleton that provides auxiliary torque to both the ankle and knee joints during the stance phase of gait in a real-world environment, using one quasi-direct-drive (QDD) motor .This lightweight exoskeleton incorporates a novel driving mechanism: the Unidirectional Ankle-Knee Gait Clutch (UAKC) , which allows for the sequential provision of auxiliary torque to the knee and ankle joints during the stance phase of gait. We trained a lightweight convolutional neural network to determine gait phases from scanned insole pressure data and generate corresponding biological torques. We provide a detailed exposition of the design concept and operation of the lightweight exoskeleton. Through a series of experiments, we evaluated the performance of the lightweight exoskeleton. In real-world conditions, it reduced human energy consumption by 8.9±1.3% compared to walking without the exoskeleton.This study reports on the potential of this rigid-cable coupled underactuated exoskeleton in enhancing human movement.**

***Index Terms*—Wearable robotics, exoskeletons , QDD , sequential assistance.**

I.INTRODUCTION

LIGHTWEIGHT,highly flexible, and easily portable lower limb exoskeletons hold immense potential for restoring mobility and enhancing human functionality. Over the past two decades, various types of lower limb exoskeletons have emerged to aid patients or augment human motor capabilities [1]-[4]. Among them, the most outstanding performances can be broadly categorized into two types: one type consists of exosuits composed of fabric and cables. These exoskeletons are soft, lightweight, and can effectively provide assistance to the human body. They are also more readily accepted in appearance. The actuators in these exoskeletons are often positioned far from the point of interaction with the human body, and in some cases, the actuators are even placed externally. For example, Asbeck et al. [3] studied a exosuit with the drive motor located at the waist and the point of action at the ankle. Witte et al. [5] placed the actuators on a fixed testing platform in order to minimize the impact of the actuator's mass. However, these soft exoskeletons face challenges such as limited load-bearing capacity and reduced stability.

Another category involves rigid exoskeletons powered by QDD motors. Current research has explored the application of QDD motors for individual joints in lower limb exoskeletons, such as the ankle exoskeleton proposed by Slade et al. [6], the hip exoskeleton developed by Yu et al. [7], and the knee exoskeleton developed by Huang et al. [8]. In contrast to traditional exoskeletons driven by high reduction ratio motors, these exoskeletons, employing QDD motors, exhibit significant reductions in weight and improved backdrive performance.This advancement greatly reduces the inertia of the exoskeleton.

Due to the direct application of assisting torques at the joints by the actuators in these exoskeletons, they incur lower energy losses compared to exosuits. Moreover, the simplicity of the QDD motor structure and the relatively fixed nature of its dynamic model reduce the challenges associated with accurately assisting human movement. However, the current state-of-the-art technologies in this category predominantly employ a 1 actuator-1 DoF configuration. While this configuration allows for complete assistance in individual movements, it suffers from limitations in system complexity and scalability with respect to weight [9].

To assist the lower limbs effectively, exoskeletons should follow a 'human-centric' approach, aligning assistance with the natural lower limb torques during human walking. In human walking biomechanics, the peak extension torque at the knee joint typically occurs in the first half of the stance phase, while the peak extension torque at the ankle joint occurs in the second half. Control strategies for single-joint exoskeletons often entail providing proportionally scaled biological assistance torques to the corresponding joints based on the gait cycle [10]-[13].These findings suggest the possibility of incorporating underactuation into exoskeleton devices, utilizing a single actuator for sequential assistance to the knee and ankle joints. Compared to the 1 actuator-1 DoF approach, this configuration reduces the number of actuators, leading to a simpler mechanical and control design [14].

Current underactuated exoskeletons are heavy and complex, mostly focusing on the hip and knee regions [15]-[16]. Asbeck et al. and Quinlivan et al. [17]-[18] developed exosuits for simultaneous assistance to ankle and hip joints during walking, but such assistance is either simultaneous or symmetric. Ma et al. [19] introduced an

This work was supported by the National Key Research and Development Program of China under Grant 2023YFC3604903, and in part by the Shanxi Provincial Key Research Project under Grant 2020XXX001, and in part by the Shaanxi Provincial Key R&D Program under Grant 2024NC-YBXM-192 ,2023-YBGY-355,2023-YBGY-356 and 2022SF-352. (Corresponding author: Aibin Zhu and Xiao Li)

[1]Xinyu Wu, Aibin Zhu,Bingsheng Bao,Jing Zhang are with the Institute of Robotics & Intelligent Systems, Xi'an Jiaotong University, Shaanxi Key Laboratory of Intelligent Robots, Xi'an 710049, China. (e-mail:wxy0614@stu.xjtu.edu.cn ;xinyuwu0614@163.com ;abzhu@mail.xjtu.edu.cn;).

[2]Diyang Dang,Lei Shi are with the Sports Center, Xi'an Jiaotong University, Xi'an 710049,China (email:382132184@qq.com; shilei@xjtu.edu.cn).

[3]Xiao Li is with Department of Rehabilitation,Senior Department of Orthopedics,the Fourth Medical Center of PLA General Hosptial,Beijing,100048,(e-mail:lixiaoPLA@163.com).

[4]Peng Xu is with Xi'an Honghui Hospital, Xi ' an 710054,China (email:xupeng_honghui@163.com)

Copyright ©2024 IEEE

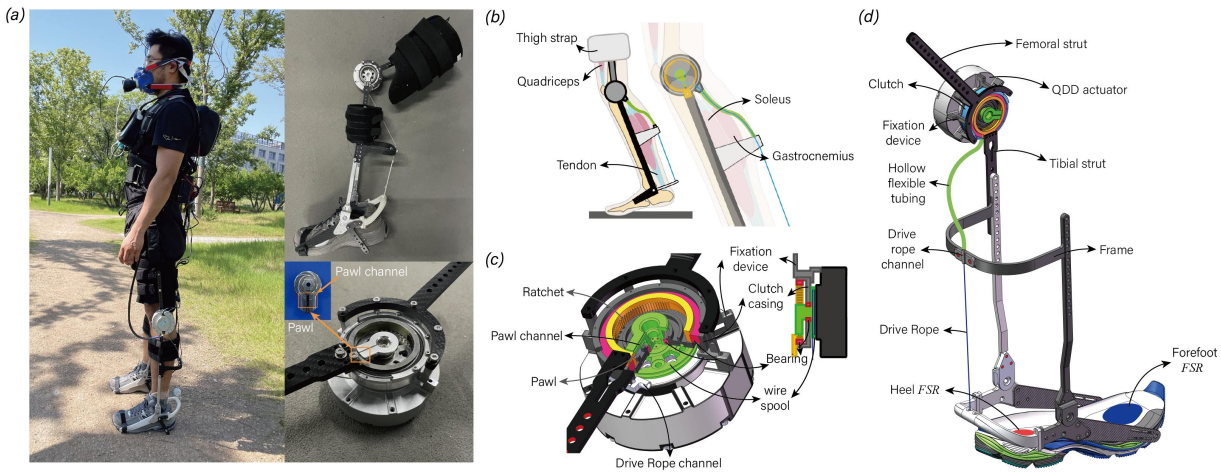

Fig.1. Ankle-Knee Powered Exoskeleton Design. (a) Actual structure of the ankle-knee co-driven exoskeleton with a unidirectional gait clutch. (b) Compared to the motor-driven knee exoskeleton, the unidirectional ankle-knee gait clutch allows the motor to sequentially allocate auxiliary torque to the knee and ankle joints. The exoskeleton acts in parallel with the quadriceps, soleus, and gastrocnemius on the human skeletal structure. (c) The clutch housing (dark gray) is rigidly connected to the motor housing. The motor output shaft is rigidly connected to the ankle joint pulley (green), and the ratchet groove (green) via bolts, and meshes with the ratchet wheel (orange, rigidly connected to the tibial structure) during ankle plantar flexion, driving the knee joint. During ankle dorsiflexion, it disengages from the ratchet wheel, driving the ankle joint. Bearings (red) support the clutch housing, ratchet wheel, and ratchet groove, allowing independent movement in the disengagement area without interference. (d) Mechanical structure of the ankle-knee-powered exoskeleton. The drive line is connected to the heel via a drive line groove .

exosuit transmitting assistance torques to the knee during flexion and to the ankle during full extension, providing sequential assistance. However, the elongated power transmission path in this mechanism may cause assisting force losses.

In this study, we introduce an underactuated lower limb exoskeleton utilizing a QDD motor to drive the system. The motor is connected to a unidirectional ankle-knee gait clutch, supplying assisting torque to the knee during the stance phase when the knee is flexed and to the ankle when dorsiflexed. A lightweight one-dimensional CNN serves as the motor controller for precise lower limb assisting torques. In the subsequent sections, we outline the mechanical structure of the proposed exoskeleton, its synchronization with gait phases, and the motor specifications. Additionally, we elaborate on the offline optimization process for the deep learning model. Finally, we showcase the exoskeleton's performance by evaluating its impact on wearer metabolism and lower limb muscle activation during real-world walking.

II.System Design

We designed a compact clutch (Figure 1) based on the kinematic characteristics of the lower limb ankle and knee joints during human walking. Unlike traditional exoskeletons with a single driver and driven joint, we serially connected the clutch to the motor's output end. This setup allows a single motor to sequentially assist the knee, then the ankle joint. In the first half of the stance phase, the motor's torque extends the flexed knee joint. During the transition from plantarflexion to dorsiflexion in the second half, the motor's torque assists in dorsiflexing the ankle joint (already in dorsiflexion).

A. Design of Lightweight Ankle-Knee Power Exoskeleton

We developed a lightweight ankle-knee power exoskeleton, driven by a QDD motor (Figure 1). It comprises three main sections: the thigh, driving unit, and ankle. The thigh section is attached to the human thigh using a 3D-printed brace secured to the waist with non-elastic nylon straps. The driving unit consists of a QDD motor (Go1, Unitree Technology, China) with a reduction ratio of 1:6.33, providing a peak torque of 23 Nm and low reflected inertia. The motor connects to the ankle joint pulley of the clutch. The ankle section is driven for dorsiflexion by the clutch's cable, simultaneously extending the shin rod through the clutch's ratchet mechanism. To reduce weight, the clutch is mainly constructed from lightweight aerospace-grade aluminum alloy, with connecting components made of carbon fiber. The ankle section design follows the approach in [23], also utilizing aerospace-grade aluminum alloy with fiberglass-reinforced nylon at the connection points to the athletic shoe and heel. The individual exoskeleton weighs 1.4 kg (motor: 0.53kg, UAKC:0.047kg excluding control computer and battery) .

We employed a portable computer (IPC-Z13, Advantech, China) to process real-time data from the plantar force-sensitive resistors (FSR406, RunesKee, China) (as shown in Figure 1d, sampled at a frequency of 200Hz), conduct real-time inference, and generate real-time lower limb ankle-knee joint biological torques. These torques were transmitted to the motor driver using the RS485 communication protocol, where the motor driver proportionally converted them into corresponding currents to drive the ankle-knee dual joints. The onboard computer, with a weight of 0.75kg, and the battery, weighing 0.3kg, resulted in a total weight of approximately 1.1kg for the waist module.

B. Detailed Operational Process of the UAKC

The operational process of the clutch within a single gait cycle is illustrated in Fig. 2(a). In Phase I, when the heel touches the ground, the corresponding leg is in the final phase of the swing phase, during which the exoskeleton does not provide any assisting torque. In Phase II.1, the corresponding leg enters the stance phase, with an increasing flexion angle at

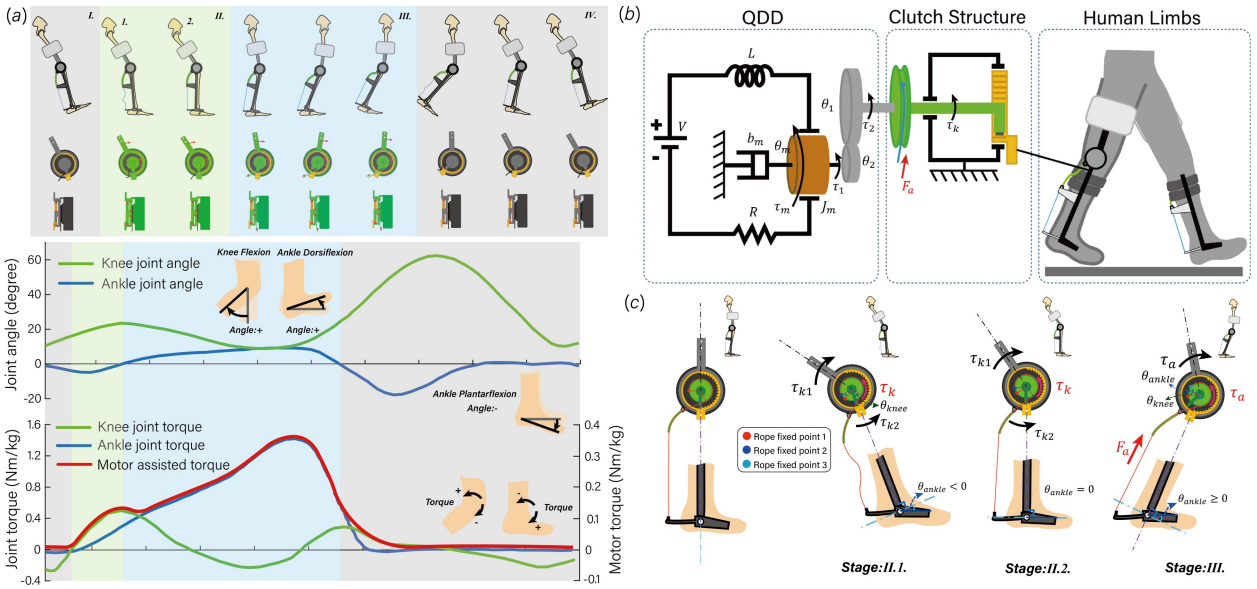

Fig.2. Detailed Operation of the Unidirectional Ankle-Knee Clutch. (a) The motor drives the knee and ankle joints sequentially within one gait cycle. The green background represents the knee joint phase, while the blue background represents the ankle joint phase. In the motor schematics, parts marked in green indicate torque applied by the motor, and red arrows represent force direction. In Phase II, the line rope is not subjected to motor torque (black), and in Phase III, the ratchet is not subjected to torque (yellow). The red torque curve in the figure represents the reference torque curve generated by the exoskeleton. (b) Human-knee joint exoskeleton coupling model, including QDD actuator, clutch, and human limb. (c) Three states of clutch operation during motion. The leftmost image represents a static standing state, Phase II.1 represents knee actuation, Phase II.2 represents a critical state, and Phase III represents ankle actuation.

the knee joint and plantarflexion at the ankle joint. The tension in the cable driving the ankle joint slackens, causing the pawl to engage with the ratchet. The motor torque is then transmitted through the pawl-ratchet mechanism, acting on the knee joint.

In Phase II.2, the knee joint reaches its maximum flexion, and the ankle joint rotates from plantarflexion to a neutral position (foot dorsiflexed at 90 degrees to the shin). At this point, the cable driving the ankle joint is fully taut. However, due to the continued engagement of the ratchet and pawl, the motor torque still acts on the knee joint through the pawl-ratchet mechanism. In Phase III, the ankle joint begins dorsiflexion, leading to the disengagement of the pawl and ratchet. The axis where the pawl is located is rigidly connected to the motor output shaft, disconnecting from the ankle joint's line pulley as the pawl moves with the ankle joint, allowing the ratchet to disengage. At this stage, the motor torque is applied to the ankle joint through the cable until the toes leave the ground, entering Phase IV - the swing phase, during which the motor operates in zero-torque mode.

The output torque exerted on the human body is sequentially distributed to the knee and ankle joints through the clutch, as depicted in Figure 2(b). The motor torque τ_m is generated by the current i, with the motor torque constant denoted as k_t

$$\tau_m = k_t i \tag{1}$$

Due to the inherent inertia of the motor rotor and assembly-induced friction, the motor output torque τ_1 can be expressed as:

$$\tau_1 = \tau_m - J_m\ddot{\theta}_m - b_m\dot{\theta}_m \tag{2}$$

Where b_m represents the viscous friction damping coefficient of the motor rotor, J_m denotes the moment of inertia of the motor rotor about its axis of rotation, and θ_m signifies the motor angle. The torque τ_1 generated by the motor is amplified to τ_2 through the reducer.

$$\tau_2 = nk_t i - n(J_m\ddot{\theta}_m + b_m\dot{\theta}_m) \tag{3}$$

In the equation, n represents the reduction ratio of the gearbox, and τ_2 denotes the output torque of the QDD actuator. The output torque of the QDD actuator is divided into two stages: knee and ankle. The segmented model is summarized in equation (4), using the ankle joint angle as the boundary, defined as zero:

$$\tau_2 = \begin{cases} \tau_k, \theta_{ankle} < 0 \\ \tau_a, \theta_{ankle} \geq 0 \end{cases} \tag{4}$$

The torque generated at human joints corresponds to each phase of the gait cycle. Our exoskeleton provides assisting torques to the lower limb joints based on the phases of the human gait cycle. The profiles of the assisting torques are derived from an open-source dataset [13], using the average data from one participant walking on level ground. The fitting is achieved through the summation of univariate Gaussian functions [20]-[23]. Given the current gait phase, denoted as x, motion-pattern-specific shaping constants (a, μ, and σ) are manually adjusted to represent a smooth synthesized ankle-knee joint torque curve based on the biological ankle-knee joint torques.

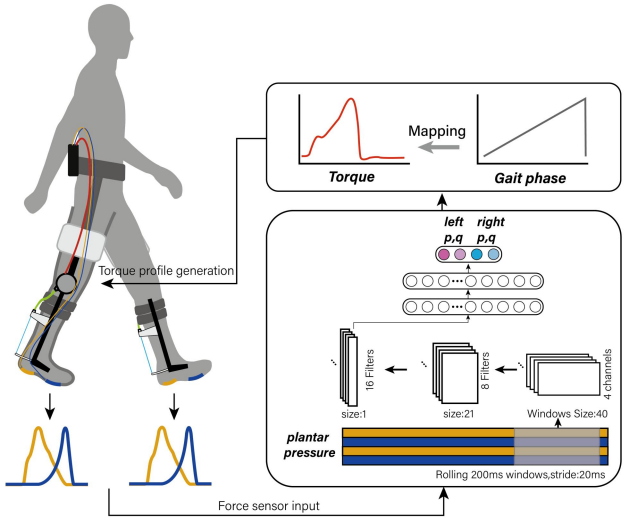

Fig.3. Phase-based Biomechanical Torque Controller. Time-series data from the insole is read with a defined window size and a certain step size. This data is then mapped to the corresponding gait phase through two convolutional layers and two fully connected layers. Based on the current gait phase, the corresponding biomechanical torque value is output.

$$\tau_2 \approx nk_t \sum_{i=1}^{n} a_i N(x, \mu_i, \sigma_i) \tag{5}$$

The Gaussian distribution N is defined as:

$$N(x, \mu, \sigma) = e^{-\frac{1}{2}(\frac{x-\mu}{\sigma})^2} \tag{6}$$

The trajectory of auxiliary torque generated by the exoskeleton actuator is determined by the current phase of gait.We scaled the peak assisting torque to 18 Nm by adjusting the amplitude coefficient (a).

III.CONTROL STRATEGY

We trained a deep learning model based on a one-dimensional convolutional network to serve as the controller for the exoskeleton. This controller can output the current gait phase of the user based on the current user's plantar pressure data. Subsequently, the exoskeleton generates corresponding joint torques based on the current user's gait phase. In the following sections, we will first describe the collection of the training dataset, followed by data annotation, and finally, the offline optimization of the model.

A. The collection of training data

Nine healthy subjects participated (gender: two female, seven male; age: 25 ± 2 years; height: 1.72 ± 0.05 m; mass: 76.1 ± 3.3 kg) in our data collection. This study was approved by the Review Committee of Xi'an Jiaotong University, and all participants provided written informed consent before participation. Plantar pressure data were recorded while subjects wore the exoskeleton and walked on a treadmill at fifteen different speeds, ranging from 0.78 to 1.48 m/s with an increment of 0.05 m/s.

Throughout the data collection process, the exoskeleton was set to output a lower constant extension torque (0.05Nm) to ensure that the clutch pawls could return to their original position after being stretched during ankle dorsiflexion. The onboard sensors of the exoskeleton (plantar pressure sensitive resistors) data were recorded at a sampling frequency of 200 Hz.

B. Ground Truth Labeling

We used heel contact information from Force Sensitive Resistor (FSR) sensors to label the ground truth gait phases. One complete gait cycle consists of two heel strikes on one side. Each rising edge of the signal represents the heel contact time. We linearly interpolated the gait phase from 0% to 100% between heel contacts, with the next heel contact returning to 0%. However, this approach led to discontinuities in the gait cycle curve, which is not conducive to the learning of deep learning models. To address this discontinuity issue, We adopted the approach from [10] and transformed the percentage of the gait phase into polar coordinates:

$$Percentage\ of\ gait\ phase = \frac{\theta}{2\pi} \times 100\% \tag{7}$$

$$p = \cos(\theta) \tag{8}$$

$$q = \sin(\theta) \tag{9}$$

Equation (7) represents expressing the gait phase percentage as a proportion of the angle θ between 0 and 2π. Using equations (8) and (9), the gait phase is transformed into two variables, p and q. This way, the gait phase percentage curve is transformed into a continuous curve. Without this transformation, the gait phase error before and after the heel strike would be calculated as 100%, leading to the controller generating incorrect torque values.

C. Offline Model Optimization

We constructed a simple one-dimensional convolutional network for gait phase estimation, as shown in Figure 3. The network takes inputs with dimensions of 4 channels (left/right forefoot/heel FSR values). A sliding window of size 40 data samples, with a time step of 20ms, is applied to the raw real-time data. The first layer of the network is a batch normalization layer, where the raw sensor data is normalized to zero mean and unit variance. The second layer consists of 8 one-dimensional convolutional kernels, each with a size of 20, a stride of 1, and no padding. The third layer consists of 16 one-dimensional convolutional kernels, each with a size of 21 (the window size from the previous layer), compressing the.data into a single row vector. This vector then passes through a sigmoid activation function and enters a two-layer fully connected network, each layer containing 20 neurons, using the hyperbolic tangent (tanh) function as the activation function. The model's output consists of two values, representing the Cartesian coordinates p and q of a single leg.

Our one-dimensional convolutional network model was trained using the Adaptive Moment Estimation (Adams) optimizer, with a learning rate of 0.001, a batch size of 64, and 1000 epochs of iterations. The model was trained on a laptop (Lenovo China) equipped with an RTX3070 (NVIDIA USA)

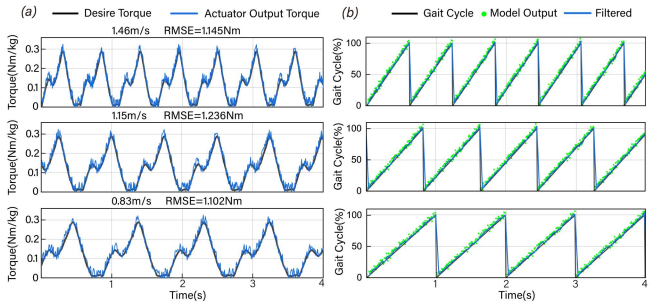

Fig.4. Performance of the Exoskeleton Controller at Slow, Normal, and Fast Walking Speeds. (a) Required auxiliary torque curve (black) and the actual output of the auxiliary torque by the controller (blue). (b) Actual gait cycle during user-worn exoskeleton walking (black), real-time generated gait cycle estimation by the model (green dots), and filtered gait cycle estimation (blue)

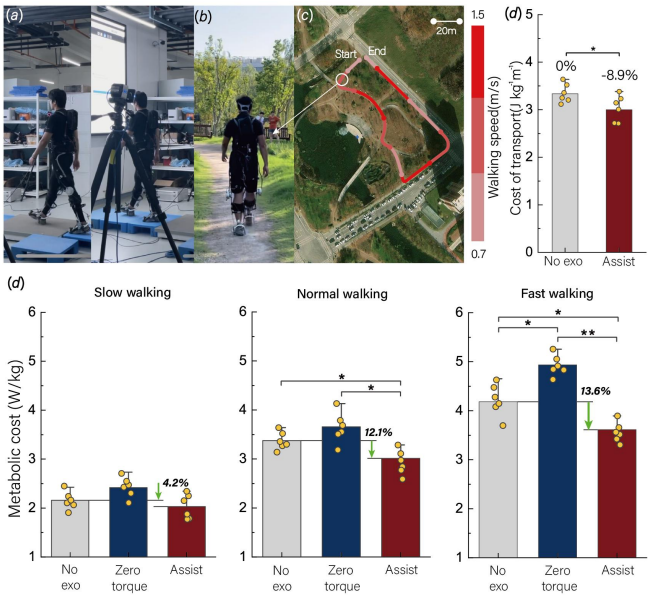

Fig.5. Joint dynamics testing and the exoskeleton's assistance effects in outdoor environments. (a) Laboratory-based dynamic experiments.(b) Subjects walking on the designated validation route. (c) A defined path was used to validate the exoskeleton's assistive effect, with a single lap length of 246 meters, and subjects walking repeatedly within a specific speed range on the path. (d) Under natural walking conditions in the park, wearing the exoskeleton reduced energy costs compared to not wearing it (ANOVA, n=6, *p<0.05). (e) Under treadmill conditions, wearing the exoskeleton reduced the metabolic cost of walking compared to walking without it (ANOVA, n=6, *p<0.05, **p<0.01).

IV. Experimental Testing

We deployed the trained model on the exoskeleton's onboard control computer through the libtorch 1.7.0 C++ interface. The online inference deployment of the model calculated the current user's gait phase estimate based on data from FSR sensors, and transmitted the estimated torque for the current gait phase back to the exoskeleton at a frequency of 50 Hz. We recruited six new participants (gender: one female, five male; age: 23 ± 2 years; height: 1.68 ± 0.05 m; mass: 63.2 ± 7.1 kg), none of whom were included in the previous group of nine participants involved in data collection. Each new participant wore the exoskeleton for 1 hour prior to the experiment, during which data were collected. After collecting data from each new participant, the model was fine-tuned on the newly collected data. Each of the six new participants underwent the aforementioned procedure. For individuals of different heights, cable lengths were adjusted based on the participant's height.

A. Exoskeleton-assisted force

We recorded the gait cycle output by the exoskeleton deep learning model along with the torque output by the controller under treadmill conditions. We calculated the Root Mean Square Error (RMSE), Coefficient of Determination (R^2), and Variance Accounted For (VAF) between the driver's output torque and the spline torque curve (Table I) to assess the accuracy of the torque controller.

B. Metabolic Consumption and Muscle Activation Testing

Subjects walked a designated 246-meter path outdoors (see Figure 5(b)) for 20 minutes, adjusting their speed based on cues. We recorded oxygen and carbon dioxide levels with a portable metabolic system(Cortex Metamax Germany) in both exoskeleton-wearing and non-wearing states. After each state, subjects rested for 30 minutes.

In the lab, we conducted tests on a treadmill at three-speed ranges(0.83~1.46m/s), evaluating metabolic consumption and muscle activation(Noraxon Ultium USA). This was done under three conditions: without the exoskeleton, in zero-torque mode, and in assisted mode, at each of the three walking speeds.

C.Joint Kinetics

Nine motion capture cameras (VICON, UK) were used to record the trajectories of the markers on the subject's lower limbs. The plantar reaction force (GRF) of the subject during the stance phase of gait was measured using a three-dimensional force plate (AMTI, USA) at a sampling frequency of 1.2 kHz, as shown in Figure 5(a). The subjects walked in three different states: without the exoskeleton, with the exoskeleton in zero torque mode, and with the exoskeleton in torque assistance mode. Fifty trials were performed in each state. Joint torque was calculated using the OpenSim4.0 inverse dynamics model (due to the use of a single three-dimensional force plate, only one gait cycle of joint torque could be calculated for each trial). Joint power was calculated from joint torque and angular velocity.

D. Data Analysis

The data analysis was conducted using MATLAB R2020a (MathWorks, Natick, USA). Muscle activation and joint kinetics data were segmented, normalized to the percentage of the gait cycle, and averaged over the gait cycle.

Statistical significance tests were evaluated using one-way repeated measures analysis of variance (Repeated-measures ANOVA), and Tukey's test was employed for between-variable comparisons, with a significance level set at $p < 0.05$.

V. Results

A. Real-time Inference Validation

We selected a representative participant and analyzed the average assisted torque curve generated by the exoskeleton's

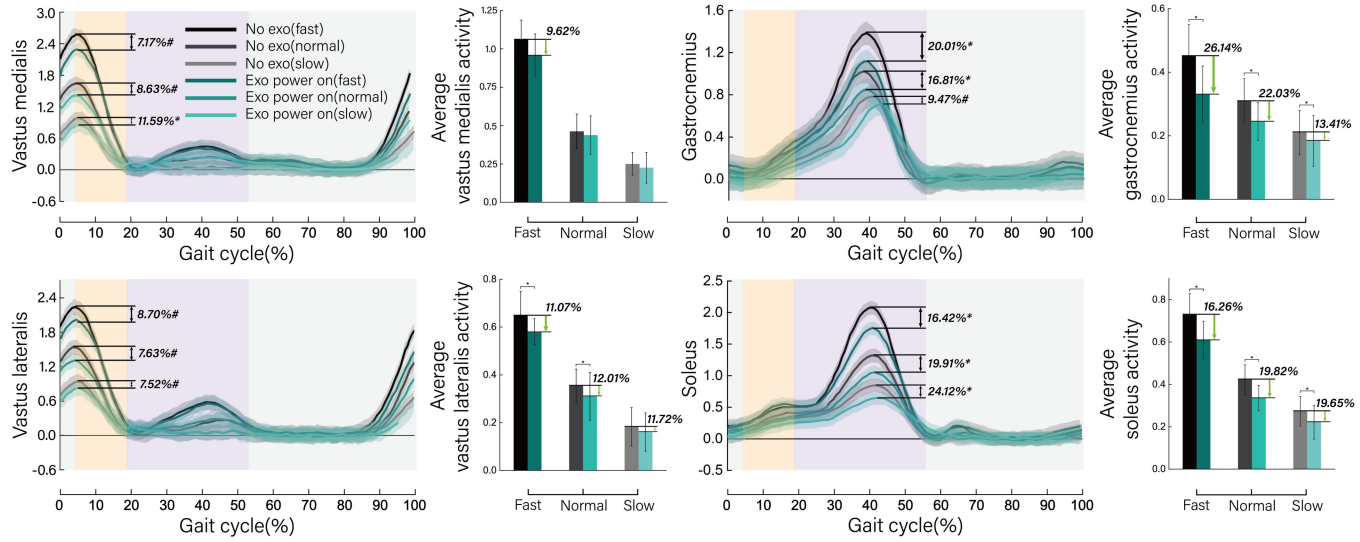

Fig.6. Electromyogram of Participants at Three Different Speeds. The muscle activations were measured in two different modes: without the exoskeleton and with powered assistance. The black curve represents muscle activation without the exoskeleton, while the green curve represents muscle activation with powered assistance. Curve colors transition from dark to light, indicating walking speed from fast to slow. Corresponding bar graphs represent the average muscle activation within a single cycle. '*' denotes a significant difference, $p<0.05$, '#' indicates no significant difference, $p>0.05$.

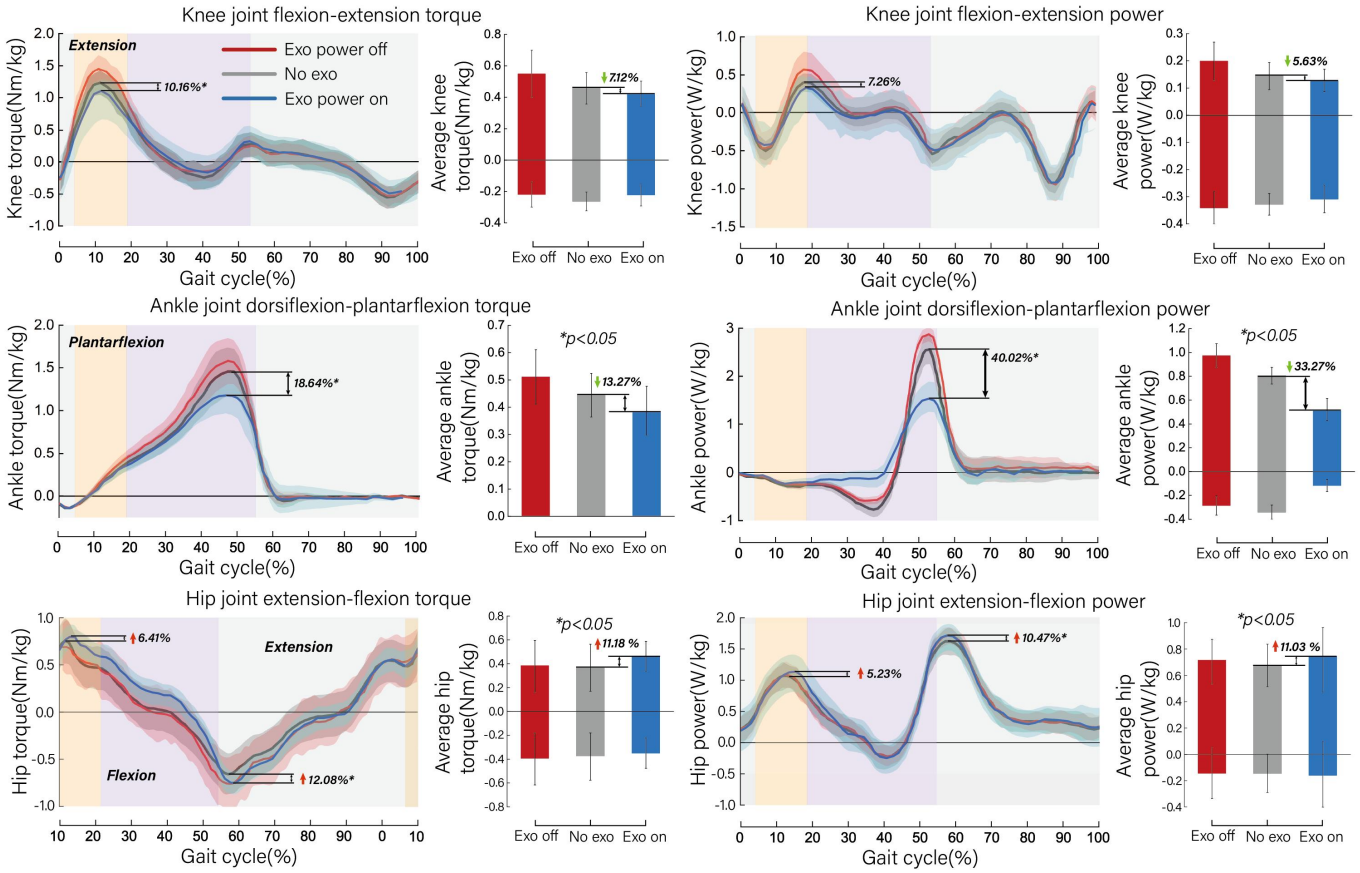

Fig.7. Average joint torque and power during level walking. The average joint torque and power of the knee and ankle joints were computed under three different modes of the exoskeleton: zero torque mode, no exoskeleton, and torque assistance mode. The red line represents the joint dynamics under the zero torque mode (human and exoskeleton work together), the value of the blue line is calculated by subtracting the auxiliary torque/power from the joint dynamics measured under the torque assistance mode (human and exoskeleton work together), and the gray line represents the biological joint dynamics under the no exoskeleton mode. The bar charts of the same color as the curves represent the average values of torque and power within a single cycle. Positive torque represents plantar flexion torque of the ankle joint (knee extension torque,hip extension torque), negative torque represents dorsiflexion torque of the ankle joint (knee flexion torque,hip flexion torque). Positive power represents joint power generation, negative power represents joint power absorption. "*" indicates significant difference, $p < 0.05$.

TABLE II COMPARISON OF PORTABLE EXOSKELETON

Exo	Actuator Paradigm	Number of Motors	Joints	Leg Weights(kg)	Waist Weights(kg)	Gear Ratio	Actuation Torque(Nm)
This work	QDD	1	Knee&Ankle	1.4	1.1	6.33:1	18
Huang[8]	QDD	1	Knee	1.4	2.1	6:1	14
Lee[12]	QDD	1	Knee	1.5	N/A	6:1	7.2
Zhu[25]	QDD	1	Knee	2.69	N/A	7:1	10.5
Slade[6]	QDD	1	Ankle	1.2	0.45	9:1	18
Taborri[2]	QDD	1	Ankle	1.3	N/A	6:1	13

biomechanical torque controller (Gender: Male, Age: 24, Height: 1.72m, Weight: 70.1kg.), as shown in Figure 4.The generated auxiliary torque exhibits two peaks, corresponding to the peak torques at the knee joint and ankle joint, respectively. The accuracy of controller output torque is shown in Table 1.

TABLE I CONTROLLER ACCURACY

Speed(m/s)	RMSE(%)	R^2	VAF
1.46	7.21	0.91	0.93
1.15	7.67	0.92	0.96
0.83	6.95	0.95	0.97

B. Walking Performance Outcomes

As shown in Figure 5, with the assistance of the exoskeleton, the energy cost of subjects walking on the designated route in the outdoor park decreased by 8.9±1.3% (ANOVA, n=6, *p<0.05). When walking on a treadmill indoors at three different walking speeds, compared to not wearing the exoskeleton, the highest metabolic consumption was reduced by 13.6±1.7% (ANOVA, n=6, *p<0.05).

Figure 6 displays EMG signals during exoskeleton-assisted walking at three speeds for four muscle groups: vastus medialis (VM), vastus lateralis (VL), gastrocnemius, and soleus. Measurements were taken without the exoskeleton. Compared to walking without the exoskeleton, fast-paced walking showed a 7.17% reduction in VM peak activation, with a 9.62% decrease in the average within a single gait cycle; VL exhibited an 8.7% reduction in peak activation and an 11.07% decrease in the average; gastrocnemius displayed a 20.01% reduction in peak activation, and a 26.14% reduction in the average within a single gait cycle; soleus demonstrated a 16.42% reduction in peak activation and a 16.26% reduction in the average within a single gait cycle.

The average sagittal plane joint torque and power for six subjects during level walking are presented in Figure 7. Comparing the states of no exoskeleton assistance to torque assistance, the knee joint exhibited a 10.16% reduction in peak biological torque, a 7.12% decrease in average torque within a gait cycle, a 7.26% decrease in peak power, and a 5.63% decrease in average power within a gait cycle. Simultaneously, the ankle joint experienced an 18.64% reduction in peak biological torque, a 13.27% decrease in average torque within a gait cycle, a 40.02% reduction in peak power, and a 33.27% reduction in average power within a gait cycle. Additionally, we observed a 6.41% increase in hip joint extension torque, and a 12.08% increase in flexion torque. The hip joint also showed a 10.47% increase in peak power and an 11.03% increase in average power.

VI. DISCUSSION AND CONCLUSION

The objective of this work is to design and test a lightweight exoskeleton that can drive both the ankle and knee joints with a single actuator, minimizing inertial costs to power more joints in real-world settings. The exoskeleton presented in this paper outperforms comparable models in key parameters (see Table II). In comparison to existing knee or ankle exoskeletons driven by 1QDD actuator-1DoF, we achieved the assistance in driving two joints while maintaining the exoskeleton weight essentially unchanged, as demonstrated in previous studies [8], [12], and in some cases, even lighter than certain exoskeleton components, as observed in [12], [25].

The primary weight reduction in our design is attributed to the introduction of a clutch mechanism to replace a QDD actuator, with the clutch weighing 0.047 kg compared to the 0.53 kg of a single QDD actuator. Material selection, emphasizing lightweight materials while maintaining structural strength, further contributed to the weight reduction. These joint efforts in design and material selection collectively achieved a lower exoskeleton weight. However, our exoskeleton remains relatively heavier compared to ankle exoskeletons proposed by Slade et al. [6] and Toborri et al. [2]. This may be attributed to the extensive use of carbon fiber in the latter, and a lower overall material consumption in the exoskeleton structure of the former. Minimizing the mass of the waist controller is also crucial; in contrast to the exoskeleton used by Slade et al. [6], the centralized electronic hardware in our work for waist control is relatively heavier, impacting wear comfort and increasing the user's physical burden.

Our research findings support the hypothesis that providing extension torques to the knee and ankle joints during the stance phase results in a reduction of biological extension torques at these joints. Figure 7 illustrates the assistance percentage. Although the actuator can stably output an assisting torque of 18 Nm (The maximum restricted torque is 18Nm, but in actual operation, the output did not reach the full extent.) ,the actual assistance percentage differs from the expected value due to the exoskeleton's self-weight, mechanical friction, and parasitic torques introduced between the exoskeleton and the human body [19].

The reactive torques of the ankle-knee exoskeleton affect the normal biological torque at the hip joint, as shown in Figure 7. Despite not being directly connected to the hip, the torques produced by the actuator are transmitted to the hip joint through straps attached to the thigh and torso. This

results in an increased torque at the hip joint during the stance phase in the exoskeleton assistance mode. In the swing phase, the attached exoskeleton adds mass, leading to an elevated hip joint torque. However, this effect is evidently inevitable, as both single-joint knee exoskeletons and ankle exoskeletons similarly influence the human hip joint.

In real-world scenarios, our exoskeleton requires further optimization compared to Slade et al.'s work [6]. We suspect that the main reasons are the weight of the control system hardware and the resulting reactive torques on the hip joint. However, compared to Lee et al.'s study [12], our approach is more effective in reducing human energy consumption. We hypothesize that this may be attributed to our ankle joint extension torque assistance, suggesting that assisting the ankle joint during human walking may be more beneficial than the knee joint.

The inspiration for this work draws from various sources, including the dynamic ankle exoskeleton proposed by Slade et al.[6], the passive ankle exoskeleton structure introduced by Collins et al.[24], and the underactuated soft exoskeleton structure for the lower limbs presented by Ma et al.[19]. In real-world conditions, human energy cost is reduced by 8.9 ± 1.3% compared to not wearing an exoskeleton. This study reports the potential of this rigid-cable coupled underactuated exoskeleton in enhancing human movement. Our future work will explore the operational states of the unidirectional ankle-knee clutch under various terrain conditions and consider the use of underactuated structures at the hip to compensate for hip joint movements.

REFERENCES

[1] K. A. Witte, J. Zhang, R. W. Jackson, and S. H. Collins, “Design of two lightweight, high-bandwidth torque-controlled ankle exoskeletons,” in 2015 IEEE International Conference on Robotics and Automation (ICRA), Seattle, WA, USA: IEEE, May 2015, pp. 1223–1228.

[2] J. Taborri et al., “RANK - Robotic Ankle: Design and testing on irregular terrains,” in 2022 IEEE/RSJ International Conference on Intelligent Robots and Systems (IROS), Kyoto, Japan: IEEE, Oct. 2022, pp. 9752–9757.

[3] A. T. Asbeck, K. Schmidt, I. Galiana, D. Wagner, and C. J. Walsh, “Multijoint soft exosuit for gait assistance,” in Proc. IEEE Int. Conf. Robot.Automat., 2015, pp. 6197–6204.

[4] B. T. Quinlivan et al., “Assistance magnitude versus metabolic cost reductions for a tethered multiarticular soft exosuit,” Sci. Robot., vol. 2, no. 2,2017, Art. no. eaah4416.

[5] K. A. Witte, P. Fiers, A. L. Sheets-Singer, and S. H. Collins, “Improving the energy economy of human running with powered and unpowered ankle exoskeleton assistance,” Sci. Robot., vol. 5, no. 40, p. eaay9108, Mar. 2020.

[6] P. Slade, M. J. Kochenderfer, S. L. Delp, and S. H. Collins, “Personalizing exoskeleton assistance while walking in the real world,” Nature, vol. 610, no. 7931, pp. 277–282, Oct. 2022.

[7] S. Yu et al., “Quasi-Direct Drive Actuation for a Lightweight Hip Exoskeleton With High Backdrivability and High Bandwidth,” IEEE/ASME Trans. Mechatron., vol. 25, no. 4, pp. 1794–1802, Aug. 2020.

[8] T.-H. Huang et al., “Modeling and Stiffness-Based Continuous Torque Control of Lightweight Quasi-Direct-Drive Knee Exoskeletons for Versatile Walking Assistance,” IEEE Trans. Robot., vol. 38, no. 3, pp. 1442–1459, Jun. 2022.

[9] E. Tricomi et al., “Underactuated Soft Hip Exosuit Based on Adaptive Oscillators to Assist Human Locomotion,” IEEE Robot. Autom. Lett., vol. 7, no. 2, pp. 936–943, Apr. 2022, doi: 10.1109/LRA.2021.3136240.

[10] I. Kang, P. Kunapuli, and A. J. Young, “Real-Time Neural Network-Based Gait Phase Estimation Using a Robotic Hip Exoskeleton,” IEEE Trans. Med. Robot. Bionics, vol. 2, no. 1, pp. 28–37, Feb. 2020.

[11] I. Kang, D. D. Molinaro, S. Duggal, Y. Chen, P. Kunapuli, and A. J. Young, “Real-Time Gait Phase Estimation for Robotic Hip Exoskeleton Control During Multimodal Locomotion,” IEEE Robot. Autom. Lett., vol. 6, no. 2, pp. 3491–3497, Apr. 2021.

[12] D. Lee, B. McLain, I. Kang, and A. Young, “Biomechanical Comparison of Assistance Strategies Using a Bilateral Robotic Knee Exoskeleton,” IEEE Trans. Biomed. Eng., vol. 68, no. 9, pp. 2870–2879, Sep. 2021.

[13] J. Camargo, A. Ramanathan, W. Flanagan, and A. Young, “A comprehensive, open-source dataset of lower limb biomechanics in multiple conditions of stairs, ramps, and level-ground ambulation and transitions,” Journal of Biomechanics, vol. 119, p. 110320, Apr. 2021.

[14] C. Della Santina, C. Piazza, G. Grioli, M. G. Catalano, and A. Bicchi, “Toward dexterous manipulation with augmented adaptive synergies: The Pisa/IIT Softhand 2,” IEEE Trans. Robot., vol. 34, no. 5, pp. 1141–1156, Oct. 2018.

[15] Y. Liu, Y. Gao, F. Xiao, and J. Zhao, “Research on the cable-pulley underactuated lower limb exoskeleton,” in 2017 IEEE International Conference on Mechatronics and Automation (ICMA), Takamatsu, Japan: IEEE, Aug. 2017, pp. 577–583.

[16] A. F. Soliman and B. Ugurlu, “Robust Locomotion Control of a Self-Balancing and Underactuated Bipedal Exoskeleton: Task Prioritization and Feedback Control,” IEEE Robot. Autom. Lett., vol. 6, no. 3, pp. 5626–5633, Jul. 2021.

[17] A. T. Asbeck, S. M. M. D. Rossi, I. Galiana, Y. Ding, and C. J. Walsh, “Stronger, smarter, softer: Next-generation wearable robots,” IEEE Robot.Automat. Mag., vol. 21, no. 4, pp. 22–33, Dec. 2014.

[18] B. T. Quinlivan et al., “Assistance magnitude versus metabolic cost reductions for a tethered multiarticular soft exosuit,” Sci. Robot., vol. 2, no. 2,2017, Art. no. eaah4416.

[19] L. Ma, Y. Leng, W. Jiang, Y. Qian, and C. Fu, “Design an Underactuated Soft Exoskeleton to Sequentially Provide Knee Extension and Ankle Plantarflexion Assistance,” IEEE Robot. Autom. Lett., vol. 7, no. 1, pp. 271–278, Jan. 2022.

[20] I. Kang, D. D. Molinaro, S. Duggal, Y. Chen, P. Kunapuli, and A. J. Young, “Real-Time Gait Phase Estimation for Robotic Hip Exoskeleton Control During Multimodal Locomotion,” IEEE Robot. Autom. Lett., vol. 6, no. 2, pp. 3491–3497, Apr. 2021.

[21] D. A. Winter, “Kinematic and kinetic patterns in human gait: variability and compensating effects,” Human movement science, vol. 3, no. 1-2, pp. 51–76, 1984.

[22] G. Bovi, M. Rabuffetti, P. Mazzoleni, and M. Ferrarin, “A multipletask gait analysis approach: kinematic, kinetic and emg reference data for healthy young and adult subjects,” Gait & posture, vol. 33, no. 1, pp. 6–13, 2011.

[23] R. Riener, M. Rabuffetti, and C. Frigo, “Stair ascent and descent at different inclinations,” Gait & posture, vol. 15, no. 1, pp. 32–44, 2002.

[24] S. H. Collins, M. B. Wiggin, and G. S. Sawicki, “Reducing the energy cost of human walking using an unpowered exoskeleton,” Nature, vol. 522, no. 7555, pp. 212–215, Jun. 2015.

[25] H. Zhu, C. Nesler, N. Divekar, V. Peddinti, and R. Gregg, “Design principles for compact, backdrivable actuation in partial-assist powered knee orthoses,” IEEE/ASME Trans. Mechatronics, vol. 26, no. 6, pp. 3104–3115,Dec. 2021, doi: 10.1109/TMECH.2021.3053226.